We are IntechOpen, the world's leading publisher of Open Access books Built by scientists, for scientists

6,900
Open access books available

186,000
International authors and editors

200M
Downloads

154
Countries delivered to

Our authors are among the

TOP 1%
most cited scientists

12.2%
Contributors from top 500 universities

CLARIVATE ANALYTICS
BOOK CITATION INDEX
INDEXED

WEB OF SCIENCE™

Selection of our books indexed in the Book Citation Index
in Web of Science™ Core Collection (BKCI)

Interested in publishing with us?
Contact book.department@intechopen.com

Geiger Avalanche Photodiodes (G-APDs) and Their Characterization

Giovanni Bonanno, Massimiliano Belluso,
Sergio Billotta, Paolo Finocchiaro
and Alfio Pappalardo
INAF - Osservatorio Astrofisico di Catania,
INFN – Laboratori Nazionali del Sud Catania
Italy

1. Introduction

In many fields and in particular in astrophysical observations, a chronic problem is the photon-starving condition, which becomes severe when images are to be obtained in short acquisition times (from micro to milliseconds), as happens in hot areas of astrophysics: optical counterparts of high-energy gamma-ray bursts, study and interpretation of Supernovae bursts. CCDs are inherently unable to provide accurate measurements of such fast low-intensity transients at high frame rates. To respond to single photons, suitable detectors must provide output signals that are sufficiently high to be individually processed by electronic circuits. Therefore, only detectors with an internal mechanism that provides a high multiplication of charge carriers are suitable, namely vacuum tube photomultipliers (PMTs), solid-state avalanche photodiodes (APDs) and electron-multiplying CCDs (EM-CCDs). In PMTs, the photocathodes available for the visible spectral range provide fairly good quantum efficiency and low noise, whereas cathodes for the red and near-infrared range have lower quantum efficiency and must be cooled to reduce the dark-count rate. PMTs are bulky, and so not suitable for assembly in large arrays, fragile, sensitive to electromagnetic disturbances and mechanical vibrations, require high supply voltages (1–2 kV) and are costly devices, particularly the high-performance models. EM-CCDs exploit an internal multiplication process to achieve sub-electron readout noise, thus being able to detect single photons. Their quantum efficiency is very high, and they are inherently suited to imaging applications. However, due to their readout technique, they cannot provide frame rates higher than a few kilo-frames per second, and cannot be used in extreme time-resolved measurements. Single photons can be detected efficiently by avalanche diodes operating in Geiger mode, known as Single-Photon Avalanche Diodes (SPADs). Avalanche photodiodes have the typical advantages of solid state devices (small size, low bias voltage, low power consumption, ruggedness and reliability, suited to building integrated systems). In the last few years, a new kind of planar semiconductor device has slowly but steadily come out, namely the silicon photomultiplier (SiPM), with promising features that, in some respect, could even replace traditional photomultiplier tubes (Kovaltchouk et al, 2005). Based on a Geiger mode avalanche photodiode elementary cell, it consists of an array of n

independent identical microcells whose outputs are connected together. The final output is thus the analog superposition of n ideally binary signals (Buzhan et al., 2003). This scheme, along with the sensitivity of each individual cell to single photons, appears to result, in principle, in the perfect photo-sensor capable of detecting and counting single photons in a light pulse. Unfortunately, this is not the case, considering that this kind of device has several drawbacks and all of them are mainly derived from its noise features; due to lattice defects and impurities in the basic material, the dark counts cannot be reduced below a given rate, and as these mainly have a thermal origin, one could be tempted to solve the problem by cooling the device itself. This works to a given extent; however, another problem sets in, namely afterpulsing, due to charge carriers trapped within the semiconductor during the avalanche signal and later exponentially released. Cooling the device results in an increase of the exponential decay constant, and therefore, the lowest operating temperature becomes a tradeoff between random thermal counts and long-lasting afterpulse counts (Ghioni et al., 1996). This could represent an intrinsic limitation to the implementation of large-area G-APD detectors, if one actually needs the single photon sensitivity. Nonetheless, the suitable use of G-APDs depends strongly on a particular application; although dark counts are a problem for low-level light applications, if there is ample light, one can set the threshold at several photoelectrons and thus suppress them. Such a tradeoff can be useful to optimize the energy resolution. Therefore, although not capable of totally replacing the traditional photomultiplier tubes, the SiPM already promises to fulfill a wide set of requirements coming from numerous applications. Thanks to its properties, the multi-element G-APD is currently promising to find widespread use in nuclear medical imaging applications like Positron Emission Tomography (PET). In this application the G-APD is usually coupled to Lutetium Orthosilicate (LSO) or Lutetium-Yttrium Orthosilicate (LYSO) scintillators which convert gamma-rays into optical photons in the blue and in the near ultraviolet wavelength ranges (Melcher, 1992).

In this chapter, we describe the single and multi-element avalanche photodiode operating in Geiger mode. Their characterization in terms of noise and Photon-Detection Efficiency (PDE) is treated in great detail together with the adopted experimental setups, partly based on optical systems i.e. light sources, filters, monochromator and integrating spheres, and partly based on typical particle counting equipments. The developed technique to obtain very accurate PDE measurements based on single photon counting with subtraction of dark noise, and avoiding as much as possible the noise contribution due to cross-talk and afterpulses is here detailed, as well as the apparatus used for charge signal measurements based on a pulsed laser system, a charge-to-digital converter (QDC) and a time-to-digital converter (TDC). Some measurements and results on various single element G-APDs and multi-element G-APDs, manufactured by different companies, are also discussed. Finally the two most known methods (photocurrent and photon counting) to evaluate the PDE are compared and a discussion on how the noise due to afterpulse and optical cross-talk may influence the measurements is also given.

2. Single element G-APD

A single element G-APD, also called Single Photon Avalanche Diode (SPAD) is essentially a p–n junction biased at a voltage above the breakdown. At this bias, the electric field is so high (higher than 3×10^5 V/cm) that a single charge carrier injected in the depletion layer

can trigger a self-sustaining avalanche and the output current rises (sub-nanosecond rise-time) to a level of milliamps. If the primary carrier is photo-generated, the leading edge of the avalanche pulse marks (with picoseconds jitter) the arrival time of the detected photon. The current continues to flow until the avalanche is quenched by lowering the bias voltage to or below the breakdown level: the lower electric field is no longer able to accelerate the carriers to impact-ionize with lattice atoms. Then the bias voltage must be restored, in order to be able to detect another photon. The circuit that performs such operations is usually referred to as a quenching circuit (Cova et al., 1996). This operation requires suitable electronics, able to:

1. sense the leading edge of the avalanche current;
2. generate a standard output pulse, synchronous with the onset of current;
3. quench the avalanche by lowering the bias below the breakdown voltage;
4. restore the photodiode voltage to the operative level.

The most commonly used circuit in studies on Geiger-mode avalanche photodiodes is the passive-quenching circuit: the avalanche current quenches itself simply by developing a voltage drop across a high-impedance load (RL > 100 kΩ). Such a circuit is very simple and can easily be employed, but sets severe limitations on the maximum admissible photon counting rate and on detector performance in general (Cova et al., 1996). In fact, it was the introduction of the active-quenching circuit (AQC) concept by S. Cova (Cova et al., 1981) that opened the way to practical application of SPADs. Many AQC types have since been reported, with circuit structure and mounting that evolved from standard NIM cards (Brown et al., 1987) to small SMT boards suitable for compact detector modules (Ghioni et al., 1996). But, if some limitation on photon counting rate and on timing response is accepted then, by using quenching resistors, many SPADs can be easily integrated in one chip and a so called multi-element G-APD can be manufactured with sensitive areas comparable to those of small photomultiplier tubes.

A schematic diagram of the AQC developed at INAF Catania Astrophysical Observatory Laboratory for Detectors (Billotta et al., 2009) is shown in Fig. 1. The G-APD is reverse biased through the cathode at $V_{break} + V_{ex}$, where V_{break} is a voltage slightly lower than the
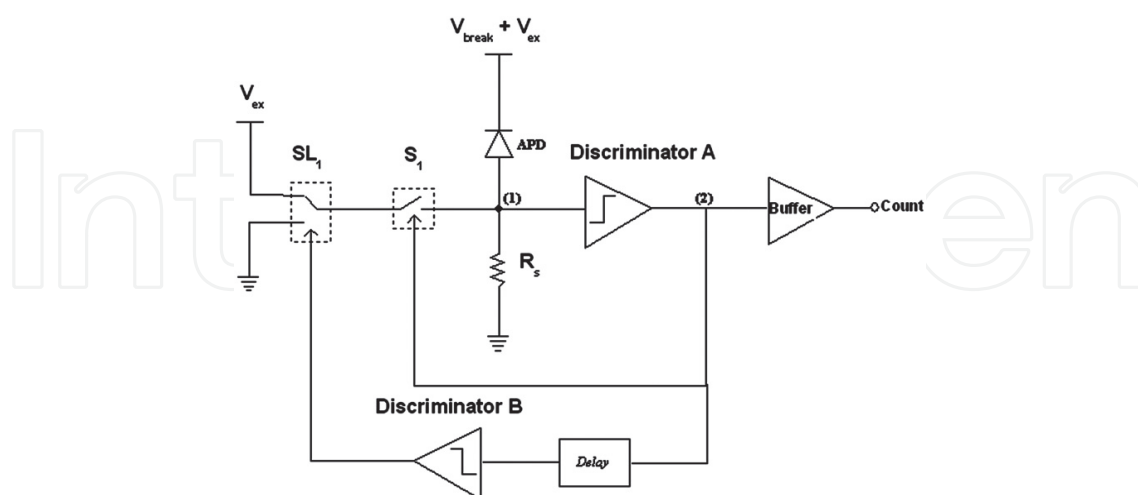

Fig. 1. The single element G-APD is biased and driven by an active quenching circuit (AQC), designed and realized at the INAF Catania Astrophysical Observatory Laboratory for Detectors (COLD), that provides for extinguishing the avalanche, bringing the SPAD to its waiting conditions and after a changeable hold-off time making the SPAD ready to detect another photon.

breakdown and V_{ex} brings the total reverse bias over breakdown. When an avalanche is triggered, the current flowing on Rs activates the discriminator A, which varies the state of node 2, giving a pulse synchronized with the avalanche. A buffer provides for the output of the pulse. Two feedback loops are used, one to quench immediately the diode to reduce the charge trapping and then avoiding afterpulses, and the other to delay the system reset, keeping quenched the diode for a dead time T known as the hold-off time. The first feedback loop acts on S_1 switch forcing the diode anode at V_{ex} voltage, giving as the total voltage V_{break} and thus leaving the diode quenched. The hold-off time is user selectable. After the time T the discriminator B by means of the switch SL_1 forces the node 1 at ground, making the SPAD ready for a new detection. At the same time the discriminators A and B open S_1 and switch SL_1 to V_{ex}.

A sketch of a single SPAD with integrated passive quenching resistor, manufactured by ST Microelectronics and tested at our laboratory, is shown in Fig. 2. The voltage can be applied through the pads 1 and 3 or through the pads 2 and 3 in order to, respectively, include or exclude the quenching resistor R_L.

In Fig. 3 is shown the reverse characteristic at room temperature obtained biasing the device including (curve a) and excluding (curve b) the quenching resistor. Measured current above the BV in curve (a) is lower due to the quenching of the dark events.
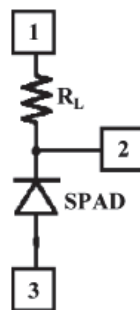

Fig. 2. Sketch of a single SPAD with integrated quenching resistor. The voltage is applied through pads 1–3 to include, or 2–3 to exclude, the quenching resistor R_L.

The plots of Fig. 3 show that the breakdown voltage is about 29.5 V, while the leakage current is few picoamps. The low value of the leakage current indicates a low generation of electrical carriers and then can be considered the first evidence of low defects of this particular kind of G-APD (Mazzillo et al.).

In order to work as a photodetector, a diode must be able to remain biased above the breakdown voltage for a sufficient time, of the order of a few milliseconds. This means that the generation–recombination phenomenon, which would trigger the avalanche, must be kept very low. Since thermally generated carriers can trigger an avalanche, it is possible to observe output current pulses also when a SPAD is kept in the dark: such an average counting rate is called dark-count rate and is one of the key parameters in defining detector noise (Ghioni et al., 1991). This aspect, as can be seen subsequently, becomes critical in multi-element G-APDs. The relevant characteristics of SPAD detectors are:

- dimensions ranging from 20 μm to 200 μm;
- dark count rates that, depending on working temperature, overvoltage and element dimensions, may vary from 20 counts/s to 1000 counts/s;

- photon detection efficiency (PDE), determined by the quantum efficiency (QE) and the trigger probability (TP), that can reach values around 60 % in the visible band.

To understand how the single element G-APD characteristics strongly depend on the bias voltage, or better, on the over voltage OV, the dark noise and the PDE are here considered. In Fig. 4 the dark noise rate of a typical device is represented as a function of OV values.
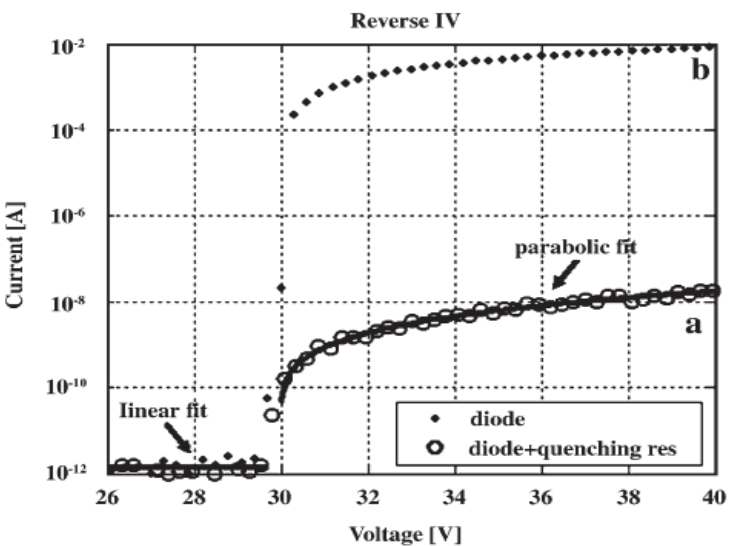

Fig. 3. SPAD reverse I–V characteristics around the breakdown voltage. (a) The quenching resistor was included. (b) The quenching resistor was excluded.
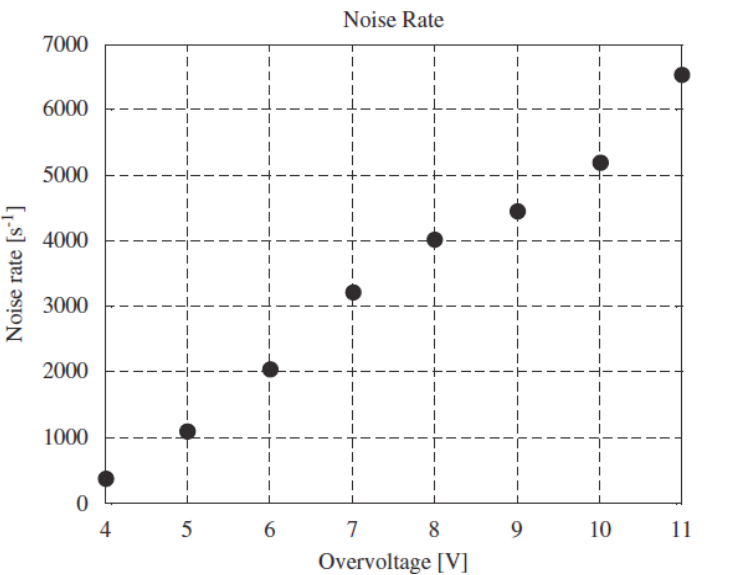
Fig. 4. SPAD dark noise rate at room temperature and increasing overvoltage.

These measurements were done at room temperature. As can be seen in Fig. 4, the dark noise rate increases almost linearly with OV. This evidence suggests that afterpulsing effects are not quite relevant also when high OV is applied to the device. In fact if afterpulsing were dominant the dark noise rate would grow steeper than linearly. Fig. 5 shows QDE (PDE with 100% of trigger probability) in the 350 ÷ 900 nm spectral range for a typical device as a function of the OV.

Both QDE curves show the same shape and reach the maximum at wavelengths between 400 and 500 nm. At 450 nm and 10 % of overvoltage we found a QDE of 30% and a QDE of 17% at 5% of overvoltage. This behavior is strictly related with the triggering probability that increases with the OV. Both QDE curves show also that biasing the device with these values, the Geiger efficiency is far from being near its maximum value, in fact the QDE scales almost linearly with the overvoltage. This means that the best operating condition will be a tradeoff between the acceptable dark count rate (that can be lowered by cooling the device) and the PDE, that of course, is preferred as high as possible. In Fig. 6 are plotted PDE values obtained from characterization of this kind of devices operated at the best condition of OV and temperature, carried out at the INAF - Catania Astrophysical Observatory (Billotta et al., 2009).
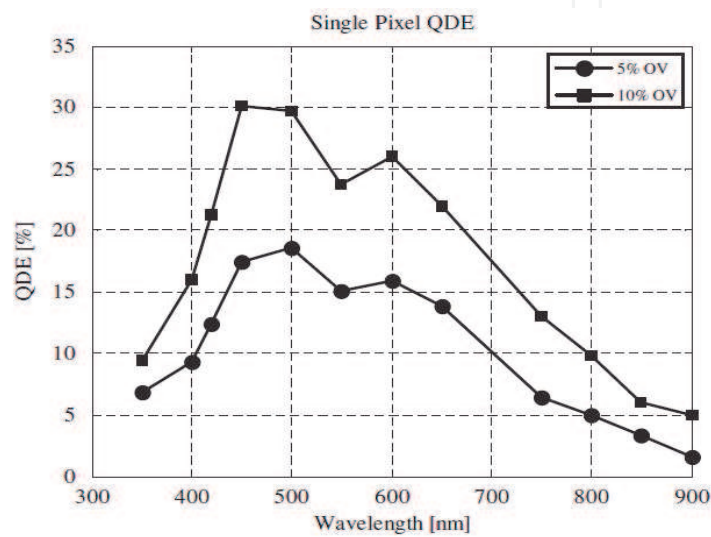
Fig. 5. SPAD quantum detection efficiency at room temperature and increasing overvoltage.
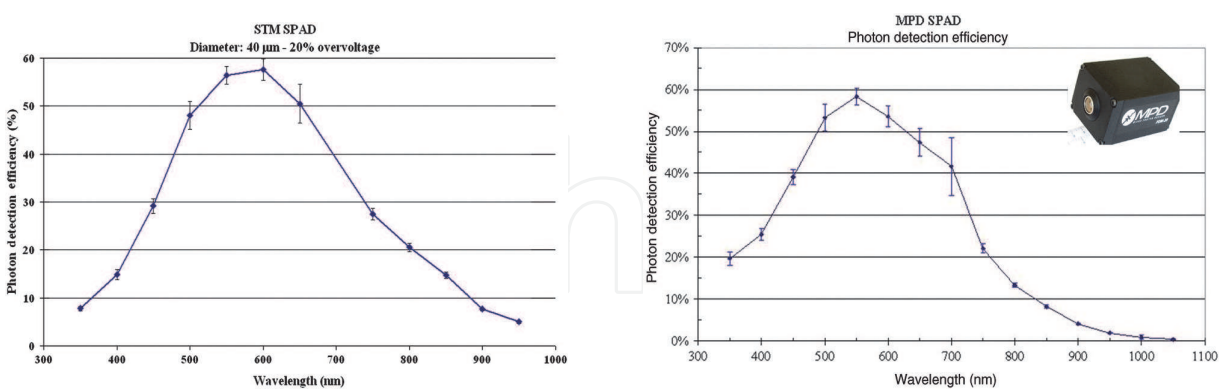

Fig. 6. (Left) PDE of a STMicroelectronics 40 μm device biased at 20% overvoltage; we can note the peak of about 60% at 600 nm. (Right) PDE of a MPD 100 μm SPADs. This device shows a PDE peak of about 60% at 550 nm.

3. Array of single element G-APD

There are applications that may require arrays of single element G-APDs. For instance, one of the toughest problems affecting ground-based telescopes is the presence of the

atmosphere, which distorts the spherical wavefront, creating phase errors in the image-forming ray paths. Even at the best sites, ground-based telescopes observing at visible wavelengths cannot achieve an angular resolution in the visible better than telescopes of 10 to 20 cm diameter, because of atmospheric turbulence alone. Adaptive optics is the answer to this problem: a deformable mirror is inserted in the light path of the telescope, and its control signal is based on measurement of the incoming wavefront, performed by a suitable high-sensitivity detector. Single element G-APD arrays can be used as curvature wavefront sensors (CWFS). By using a pulsed laser system, the array performs better than a CCD, thanks to its gating function and parallel readout, which allow faster loop cycles (Zappa et al., 2007). In Fig. 7 is shown a drawing of a planar array fabricated by STMicroelectronics (Mazzillo et al., 2007). This is manufactured by the integration of 25 pixels with a square geometry of 5 × 5.
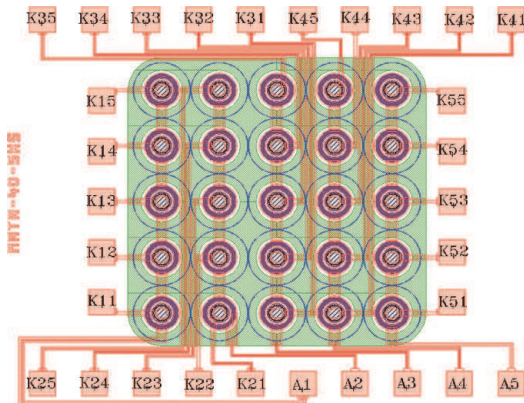

Fig. 7. Plan view of an array fabricated by STMicroelectronics. This device is manufactured by the integration of 25 pixels with a square geometry of 5 × 5.

STMicroelectronics has designed arrays with three different pixel diameters: 20, 40 and 60 mm. Separation distances between adjacent pixels are in the range of 160 and 240 mm according to different diameters. Anode contacts are in common for each row, while each cathode is separately contacted and available from outside by different pads. The typical breakdown voltage is about 30 V.

4. Multi-element G-APD

Multi-element G-APDs also known as silicon photomultipliers (SiPMs) or multi-pixel photon counters (MPPCs), have been developed during recent years as a possible alternative to vacuum photomultiplier tubes (PMT) and avalanche photodiodes (APD). A multi-element G-APD, is a photodetector constituted by hundreds to thousands of single G-APD, and the discharge is quenched by a small transparent polysilicon resistor (passive quenching) integrated on each cell's cathode. The independently operating cells are connected to the same readout line and therefore the combined output signal corresponds to the sum of all fired pixels. A schematic diagram is shown in Fig. 8.

A typical G-APD reaches an intrinsic gain for a single photoelectron of 10^6, comparable to that of vacuum phototubes (PMTs). Fig. 9 shows a G-APD of a 10 × 10 array manufactured by STMicroelectronics.

A snapshot of persistence plots taken on a digital scope is shown in Fig. 10, where the (upper plot) low-light-level pulses, generated by a laser, produce the typical equally spaced

electrical signals corresponding to discrete numbers of photons detected. The signal rise time is below 2 ns; its duration is 10 ns. The dark-count signals, shown on the lower plot, basically show up as one-cell pulses.
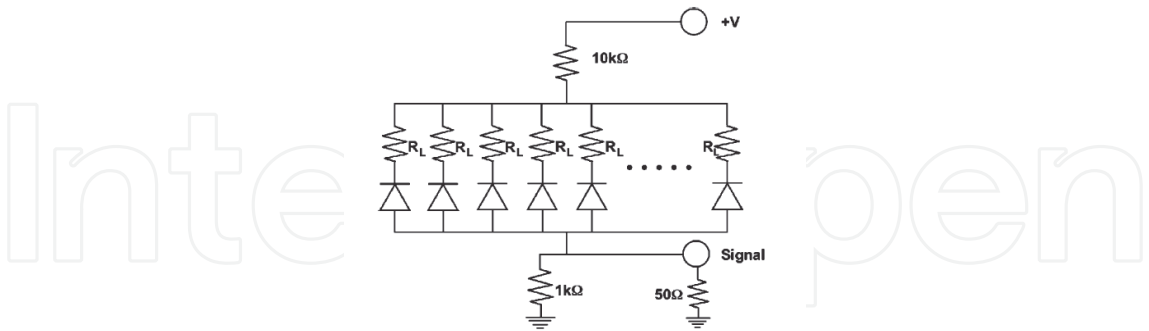

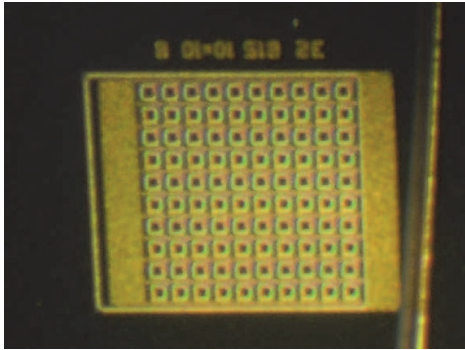Fig. 8. Electrical schematic of the SiPM, its biasing circuit, and output signal extraction.

Fig. 9. Microphotograph of the 10 × 10 SiPM with 50 μm pitch. Each cell's active area, 30 μm wide, appears in the picture as a light transparent polysilicon resistor frame surrounding a darker central spot.
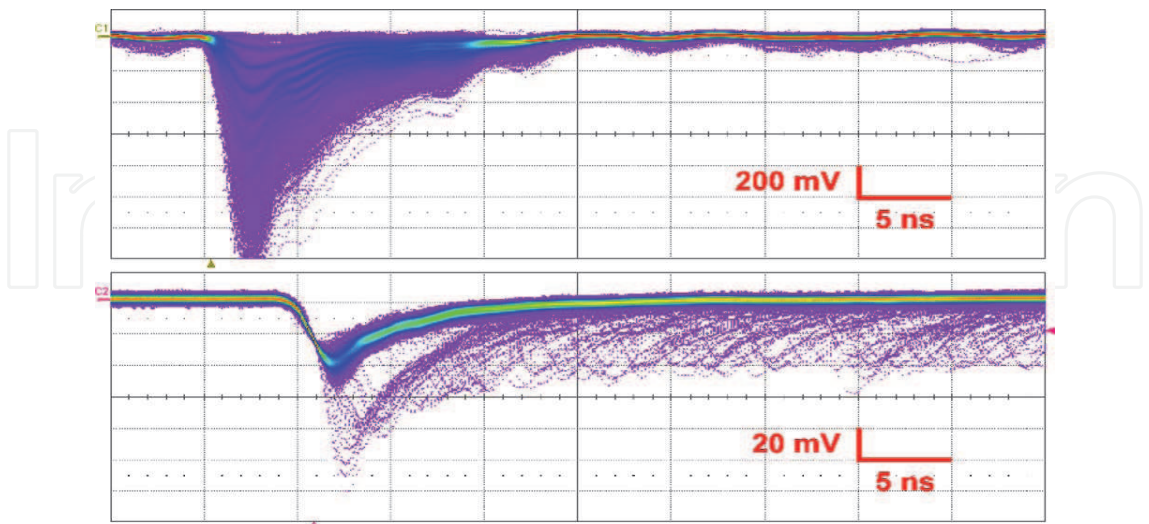
Fig. 10. Persistence plots on a digital scope of a 10 × 10 cells G-APD output signal. The upper plots is obtained by illuminating the detector with low-light-level pulses generated by a laser. The equally spaced signals correspond to discrete numbers of photons detected. The lower plot basically shows as the dark counts are due to one-cell pulse.

In multi-element G-APDs the dead area due to the quenching resistor introduces another parameter that is named "fill factor". This parameter is responsible of the lower PDE as compared to that of the single element. Indeed, as it is better explained in section 9, the PDE is the product of three factors: the quantum efficiency (QE), the trigger probability (TP) and the fill factor (FF). The electro-optical characteristics of these devices are detailed in the following sections.

5. Characterised detectors

The characterisation activity described here regards two kinds of G-APD operating in photon counting regime: SiPMs manufactured by STMicroelectronics and MPPCs manufactured by Hamamatsu. These G–APDs are biased slightly above the breakdown by an overvoltage (around 10% for the STMicroelectronics and few percents for the Hamamatsu). The passive quenching resistor is integrated on the cathode for the STMicroelectronics and on the anode for the Hamamatsu. In particular here we present the characterisation results for three G-APDs:

1. a 10 × 10 single elements (100 cells) STMicroelectronics SiPM;
2. a 10 × 10 single elements (100 cells) Hamamatsu MPPC (S10362-11-100C);
3. a 20 × 20 single elements (400 cells) Hamamatsu MPPC (S10362-11-050C).

The detectors have the following geometric characteristics:

the 100-cells SiPM manufactured by STMicroelectronics has dimensions of 0.5 × 0.5 mm^2, a pitch of 50μm and a fill factor of 36 %;

the 100-cells MPPC Hamamatsu has dimensions of 1 × 1 mm^2, a pitch of 100μm and a fill factor of 78.5%;

the 400-cells MPPC Hamamatsu has dimensions of 1 × 1 mm^2, a pitch of 50 μm and a fill factor of 61.5 %;

and the following electrical characteristics:

the STMicroelectronics SiPM has a breakdown voltage around 29.5 Volts at room temperature, with a variation coefficient of 35 mV/°C;

both Hamamatsu MPPCs have a breakdown voltage around 68.6 V at room temperature. The 100-cells MPPC has a gain G=2.4 × 10^6 (at a Bias Voltage = 69.7 V), the 400-cells has a G=7.1× 10^5 (at a Bias Voltage = 69.8 V).

Furthermore we have to note that, on the contrary of Hamamatsu MPPC, each STMicroelectronics SiPM cell is surrounded by a suitable trench filled with opaque material to avoid that photons produced during the Geiger discharge may be detected by neighboring cells. This effect is commonly named as "optical cross-talk" (Dolgoshein, 2006).

6. Experimental setups for multi-element G-APDs electro-optical parameters measurements

As written in the previous section, in this chapter we report on a complete characterisation of three different G-APDs. The purpose is to explain how accurate measurements of the relevant electro-optical parameters can be carried out to better qualify the detector performances. We measured the following characteristics:

*   dark counts, afterpulse and optical cross-talk that represent the noise sources;
*   charge response and gain;
*   photon detection efficiency (PDE).

To evaluate the above characteristics four different setups are used:

1. A counting system (for simple dark-count measurements) sketched in Fig. 11. The detector output is connected to an amplifier (a FTA810B, with gain 200 and rise time below 1ns) that produces a voltage signal, and forms the input signal of the discriminator (a Lecroy 4608) that, depending on the threshold levels generates the pulses to be counted.

2. A self-correlated timing apparatus (for afterpulse measurements) sketched in Fig. 12. The SiPM signal is acquired by the discriminator that generates two delayed signals, one to start and the other to stop the time-to-amplitude converter TAC (an Ortec 457). The TAC allows a tunable range between 50 ns and 5 µs.

3. A charge signal apparatus (for SiPM response characterization) sketched in Fig. 13. A laser (a 671 nm pulsed laser with FWHM pulse width of 40 ps), through an optical fiber, illuminates the G-APD. The G-APD output signal is connected to a discriminator (Lecroy 4608). The TTL output from the laser is used to generate the gate for the QDC.

4. An optical system (block diagram in Fig. 14) and an electronic equipment (sketched in Fig. 15) for PDE measurements. In the optical system a Xenon lamp is used as radiation source, the wavelength selection is performed by a Czerny-Turner monochromator (FWHM ≤ 1 nm in the 130–1100 nm spectral range) and a beam splitter directs the monochromatic radiation towards an integrating sphere that guarantees a spatial integration of the radiant flux on a 1 cm^2 reference photodiode (NIST traced) and on the detector to be characterized. Furthermore, we designed the detector housings, in such a way to have same aperture and distance from the centre of the sphere. The calibrated photodiode allows to evaluate the number of photons per unit area, and then, after proper rescaling, the number of photons on the detectors. The optical apparatus used for PDE measurements is one of the available facilities at "INAF-Catania" laboratory (Bonanno et al., 1996). The electronic equipment is essentially constituted by a counting system and an electrometer (Keithley 6154) that measure the photo-current from the NIST calibrated photodiode. The electrometer is connected to a PC through an IEEE 488 interface.

The actual configuration of the electronics was slightly modified and fine-tuned with respect to what is shown in the figures based on specific needs.
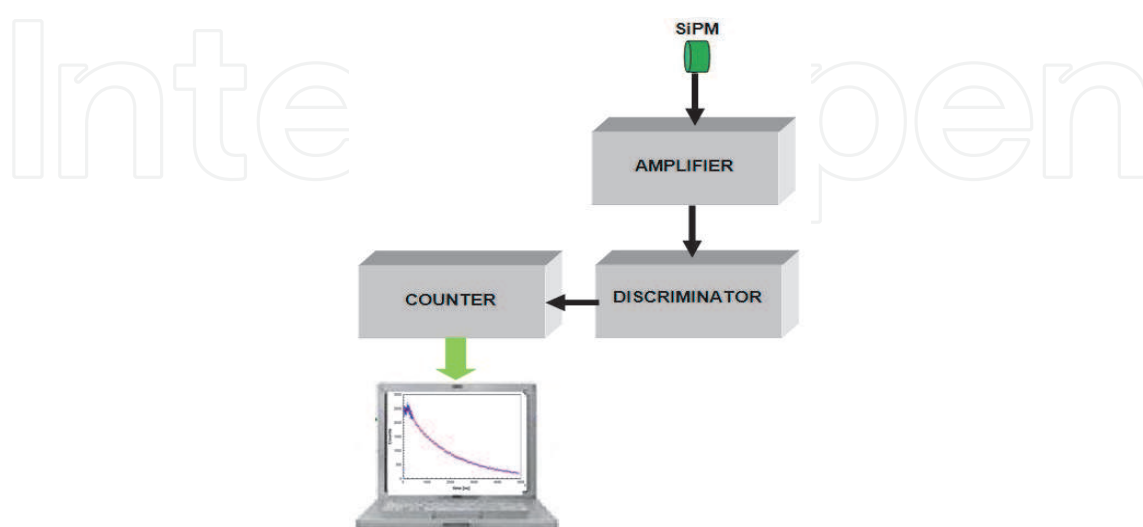

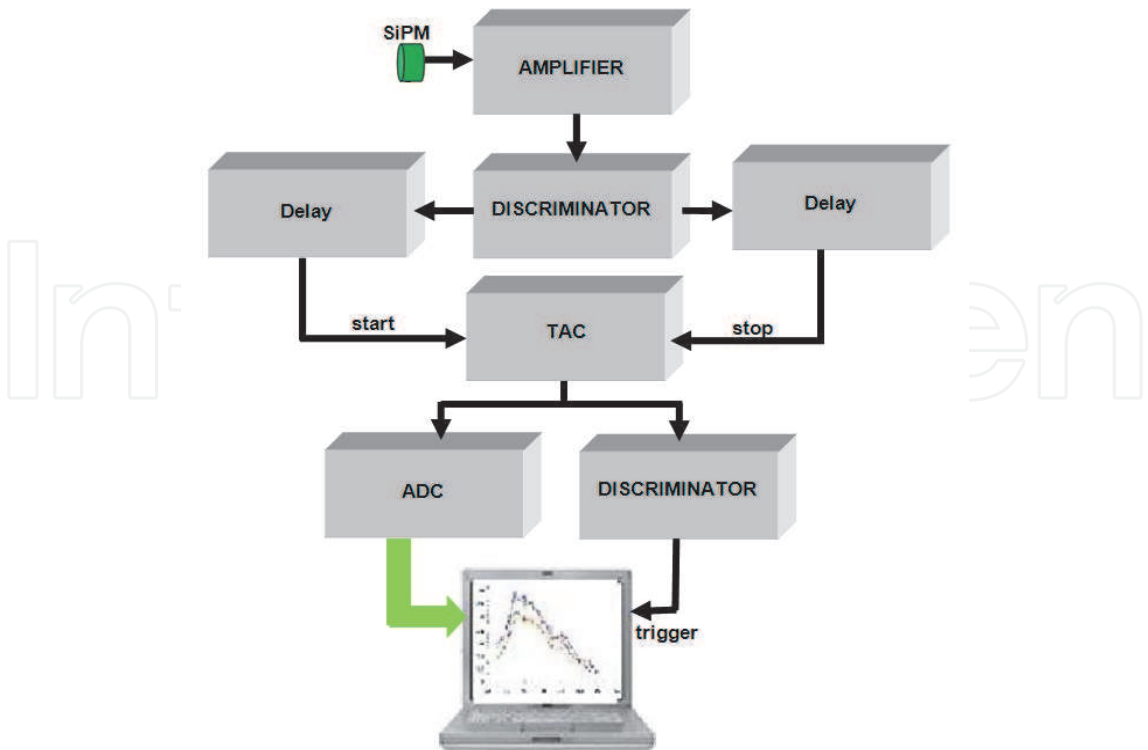Fig. 11. Sketch of the setup utilized for dark counts measurement.

Fig. 12. Sketch of the apparatus for the self-correlated timing, used for afterpulse measurements.
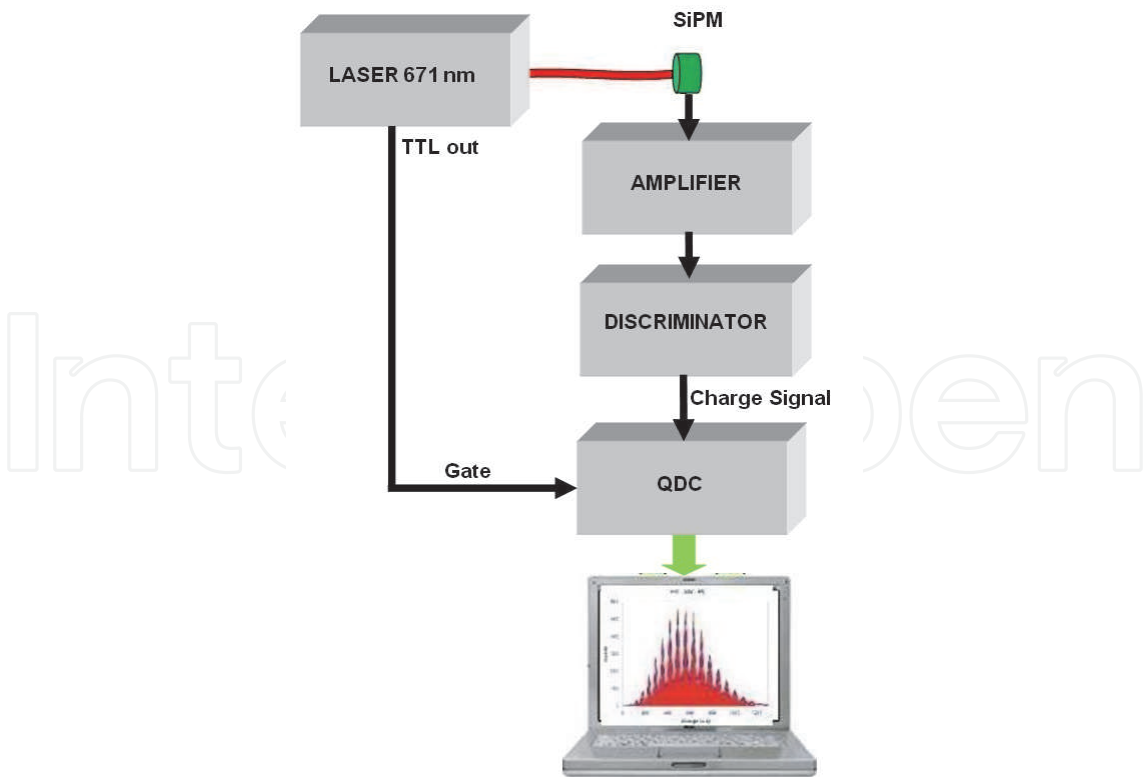

Fig. 13. Sketch of the electronics for the charge measurements used for SiPM response characterization.
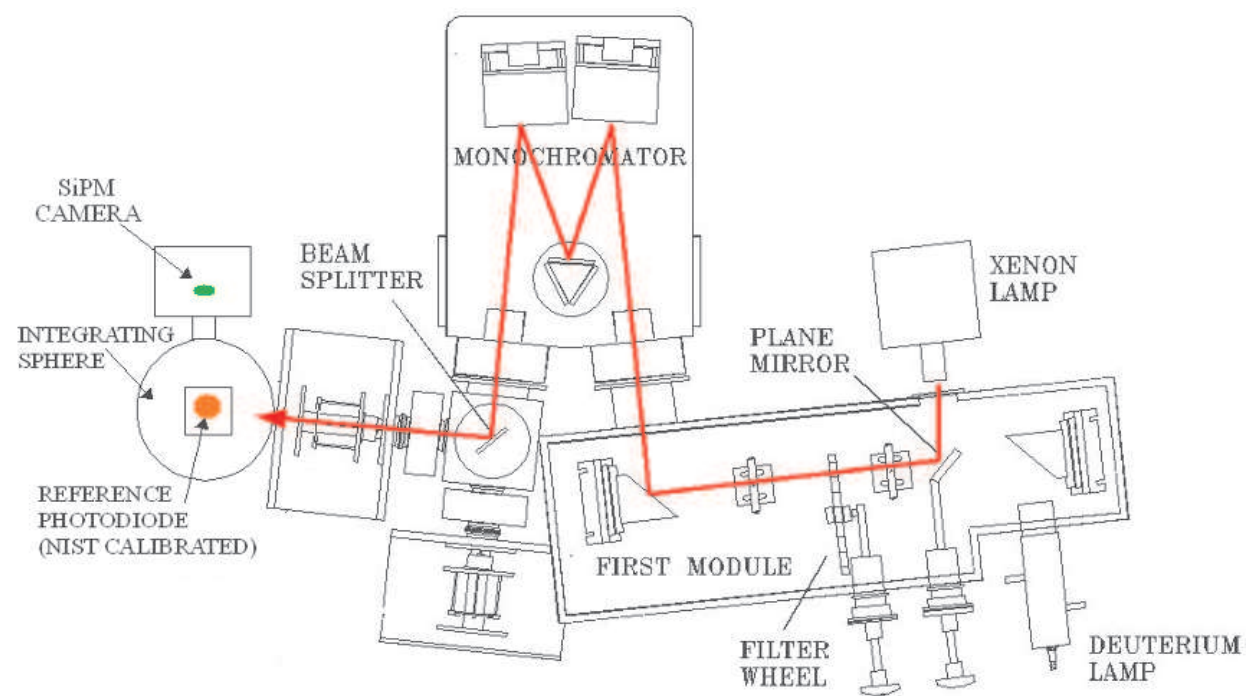
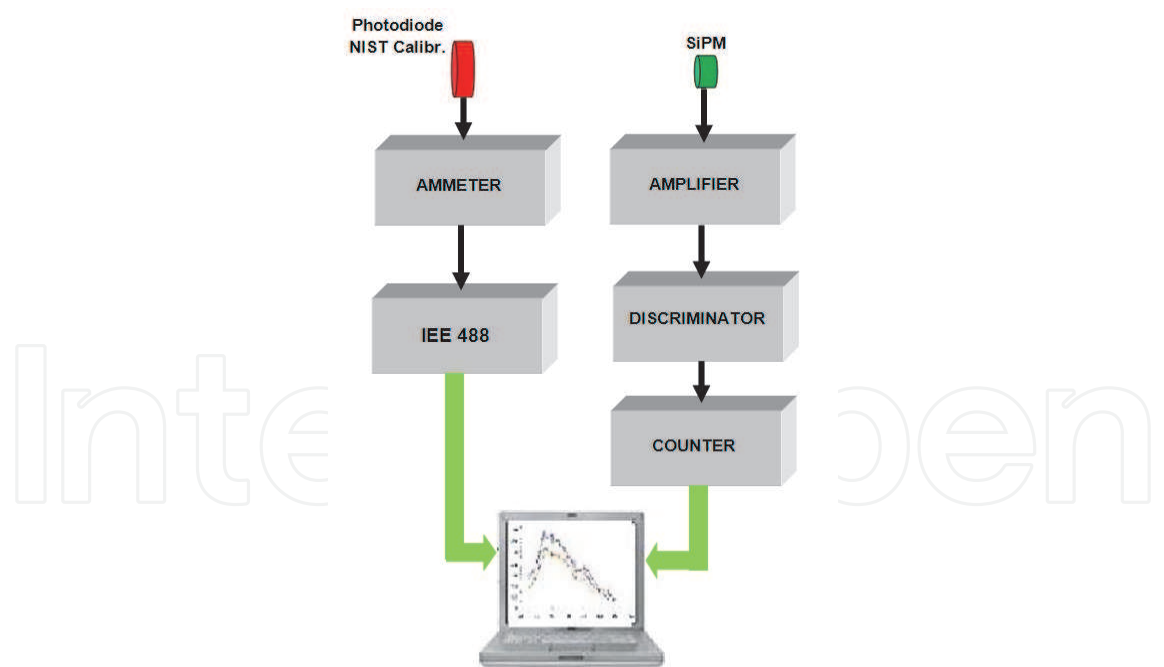Fig. 14. Schematic of the optical apparatus used for PDE measurements. The light path is also shown.

Fig. 15. Sketch of the electronics implemented for the PDE measurement.

7. Dark counts and afterpulse measurements

In order to evaluate the dark-count rate of the characterized devices, each detector is placed into a thermally stabilized light-tight box. By using the electronic setup shown in Fig. 11, the

number of noise pulses generated per unit time as a function of the discriminator threshold is measured. Fig. 16 shows the resulting plots for the G-APDs. The STMicroelectronics device is biased with a voltage of 32.5 V while the Hamamatsu device is biased with 69,7 volts. The threshold is normalized to the one-photon signal amplitude.
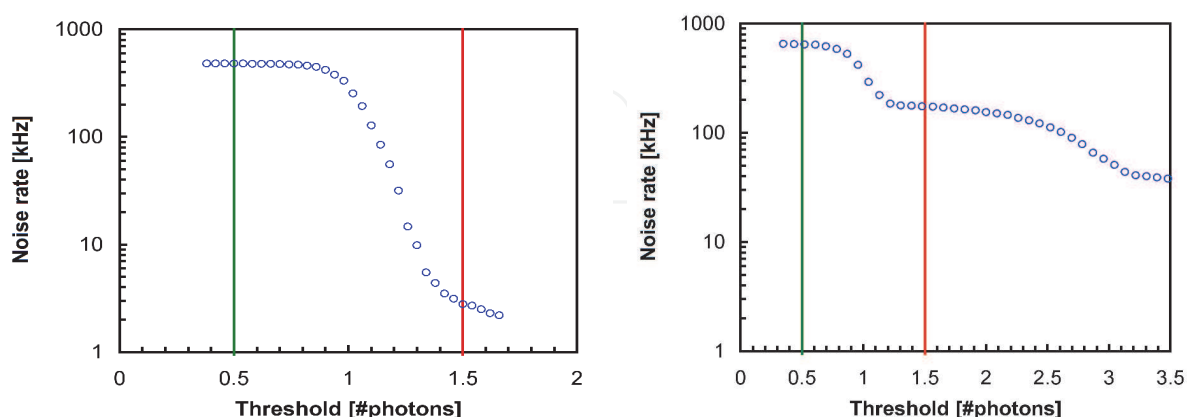

Fig. 16. Measured noise rate as a function of the discriminator threshold for the STMicroelectronics device (left), and for the Hamamatsu device (right). The noise level at 1.5 pe- is quite low for the STMicroelectronics G-APD, indicating a low level of correlated noise, while for the Hamamatsu MPPC the noise level is still considerable (also at 2.5 pe- and 3.5 pe-), confirming a non-negligible correlated noise level.

From Fig. 16 is clearly evident that even though the two G-APDs have dark noise of the same level at 0.5 pe- threshold, the noise of the STMicroelectronics device is strongly reduced at 1.5 pe- threshold. The same amount of reduction is not seen for the Hamamatsu sensor even at 3.5 pe- threshold, indicating the presence of correlated noise. A rough estimate of such correlated noise can be obtained by computing the ratio between the counting rate at 1.5 pe- and 0.5 pe- threshold. This ratio is about 0.5% for the STMicroelectronics G-APD and 27% for the Hamamatsu device. The cause of this difference is surely due to the optical trench technology adopted by STMicroelectronics that reduces considerably the optical cross-talk contribution. From these measurements rises the necessity to measure the correlated noise. An evaluation of the contribution of this noise to the real signals, can be given, for example by measuring the distribution of the time intervals between two consecutive dark pulses. For this purpose the setup sketched in Fig.12 is used. The amplified signal is passed to the discriminator, that generates two fast logic outputs that, in turn, are appropriately delayed, with one used as start and the other as stop of the TAC (Fig. 12). After a precision calibration of the time scale (Finocchiaro et al., 2008) a delay configuration is chosen to have a self-coincidence peak below the overall TAC threshold, and thus the system was only triggered whenever, following the main signal, there was another pulse between 50 ns and the full time range. In these conditions, the distribution of time intervals between two consecutive signals is measured. More details about the afterpulse noise measurement can be found in (Finocchiaro et al., 2008). In Fig. 17 can be seen the result of measurements for both G-APDs.

From Fig. 17 is evident that while the overall behavior for the STMicroelectronics G-APD is exponential, according to Poisson's law (with a small bump due to afterpulsing around 200 ns), for the Hamamatsu device we found a decreasing function with at least three exponential slopes indicating a non-random behavior.
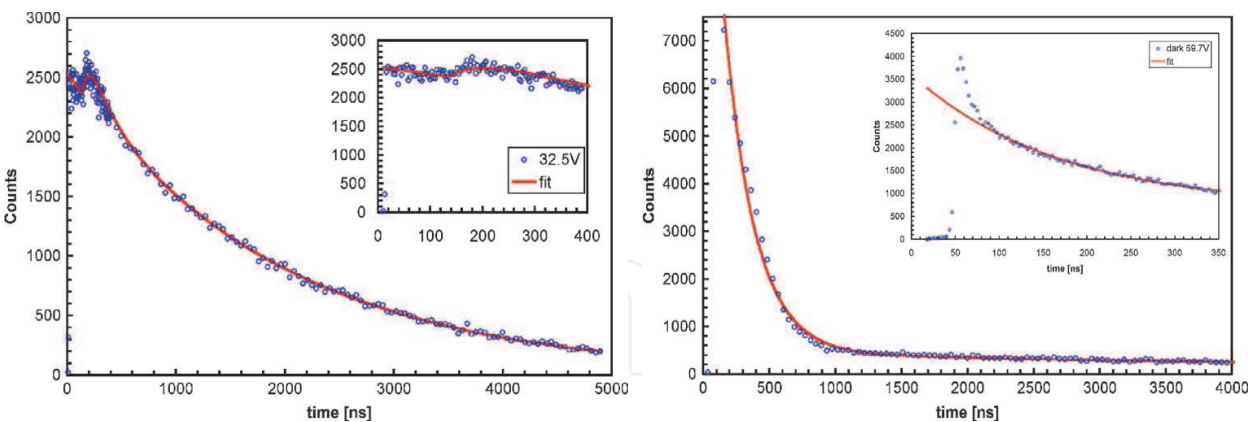
Fig. 17. Distribution of the time interval between two consecutive dark pulses for the STMicroelectronics SiPM biased at 32.5 V (left) and the Hamamatsu MPPC biased at 69.7 V (right).

8. Gain measurements

The gain measurements are of fundamental importance in computing the Photon Detection Efficiency (PDE) considered as ratio between the photo-current of the tested detector and that of the calibrated one. Uncertainties on the gain measurement directly affect the PDE values. As written in sectio n 2, each single element of the devices operates in Geiger mode, and then the interaction of one photon produces an electron-hole pair followed by an avalanche multiplication. The avalanche multiplication factor is the gain that we indicate with G, and depends on the bias voltage. For the G measurements we used the setup sketched in Fig. 13. By setting the laser intensity at various levels, the charge spectrum for each detector has been acquired. The G has been obtained by computing the average spacing between two consecutive peaks in terms of QDC channels. Values in the 10^4 to 10^5 range have been found. As an example in Fig. 18 the STM 100-cells SiPM and the Hamamatsu 100-cells MPPC charge spectra are shown.
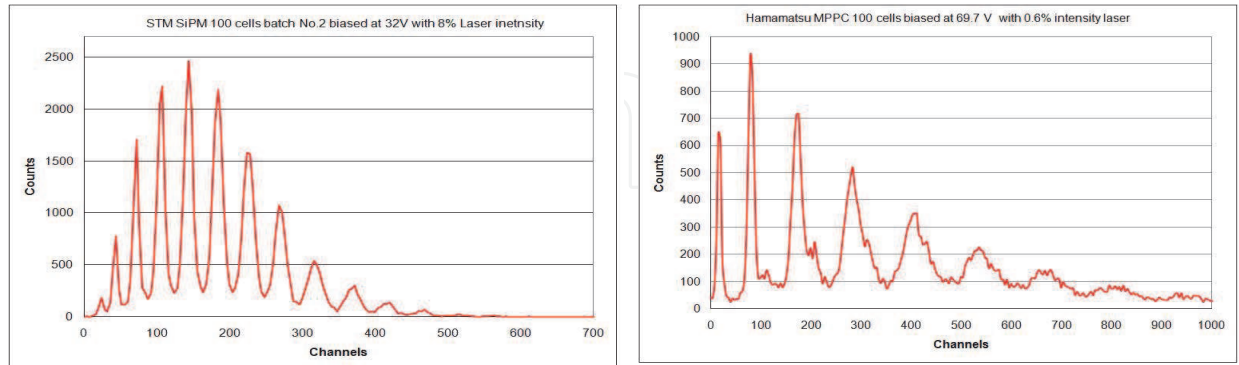

Fig. 18. On the left is plotted the charge spectrum from the STM 100-cells SiPM. On the right is the charge spectrum from Hamamatsu 100-cells MPPC.

Surprisingly for both Hamamatsu devices we have found values of G about one order of magnitude smaller than those reported on the data sheets provided with the detectors. To locate the error sources, we also checked the amplifier by using a calibrated source.

Different configurations have been investigated and some other measurements were carried out with the same results.

9. PDE measurements

Only a fraction of the photons impinging on the sensor will actually trigger an avalanche to produce a detectable signal (Piemonte 2006). Essentially three effects influence a G-APD response efficiency:

1. physical (reflection/absorption by passive layers, material), that is the so called net quantum efficiency (QE);
2. electrical (photon arrival in regions where the electric field is not suitable for triggering the avalanche), that represents in practice the probability that an event occurs and generally is named Trigger probability (TP).
3. geometrical (dead areas between cells), and is generally known as fill factor (FF);

The overall efficiency of the sensor, as for the single element, is generally named Photo Detection Efficiency (PDE), and it relates the real number of impinging photons to the measured effect (photo-electrons) and is the product of the three above mentioned effects:

$$PDE = QE \times TP \times FF \tag{1}$$

In the following sections the reader will be introduced into an important aspect to be considered when the detector PDE has to be evaluated with high accuracy. The requirement to have a well defined methodology, taking care, not only on the precision of all involved instruments, but also on the implemented procedure, is crucial to obtain precise measurements. Here we will demonstrate how the extra noise sources, optical cross-talk and afterpulse, may influence the PDE measurements. In fact, to measure the detector PDE essentially two approaches can be used:

1. one consisting in measuring the generated charges considered as current, that we name: "Photocurrent" method,
2. and another consisting in counting each produced event, that we name "Photon counting" method.

The PDE measurements for both methods have been carried out by using the optical setup sketched in Fig. 14 and the electronic setup sketched in Fig. 15.

The first consideration, to obtain accurate measurements, is addressed to the different dimensions of both detectors, the G-APD and the reference photodiode. In fact, while the tested devices have dimensions of squared millimeter, the reference detector have a sensitive area of 1 cm^2 (leakage current less than 1pA), thus in the "Photon counting" case, we have to adjust the photon flux level (from about 10^5 to about 10^7 phs·mm^{-2}·s^{-1}) in such a way that the reference detector was still sensitive and the detectors were safely in the single photon regime with negligible pile-up.

9.1 Photocurrent method

The "Photocurrent" method consists in comparing the photocurrent of the characterized detectors with respect to that of the NIST calibrated reference photodiode. In this case the setup apparatus of Fig. 15 is simplified by substituting the amplifier, the discriminator and the counter with an ammeter. In practice we have two identical systems, one for the tested and one for the reference detector, and simply we have to do measurements of the photo-generated current in both sensors. The following formula explains how the method works:

$$\text{PDE} = \left[\left(I_{\text{Det}} - I_{\text{DarkDet)}}\right) / \left(I_{\text{PhD}} - I_{\text{DarkPhD}}\right)\right] \times G^{-1} \times \text{PDE}_{\text{PhD}} \times \left(A_{\text{PhD}} / A_{\text{Det}}\right) \tag{2}$$

Where I_{Det}-I_{DarkDet} is the current measured in the tested detector, I_{PhD}-I_{DarkPhD} is the current measured in the calibrated photodiode, G is the gain (N_{el}/pe-), PDE_{PhD} is the PDE of the calibrated photodiode and A_{PhD}/A_{Det} is the detectors area ratio.

We operated the detectors at room temperature and measured the PDE of the STM SiPM biased at 32.5V (10% OV) and that of the 100 and 400 cells MPPC biased respectively at 69.8V (~2% OV) and at 69.4V (~2% OV). Using the G values obtained with our measurements, we found unreasonable PDE values (higher than expected). Thus, the sole alternative we had was using the G values given by the manufacturers. Despite a sort of uncertainty of the method, due to the fact that we have to rely on manufacturer's measurements accuracy, we decide to compute the PDE. We made the PDE computation only on the two Hamamatsu MPPCs. The obtained values are plotted in Fig. 19.

As expected the PDE of the 100 cells MPPC at 450 nm has a peak of about 50%, while the 400 cells MPPC has a peak of 30% because of the different fill factor. Now we have to investigate if these results are realistic or the noise contribution has to be taken into account and avoided as much as possible. It is clear that a technique, based on photocurrent measurements, is unable to discriminate from extra-generated pulses, i.e. afterpulses and optical cross-talk pulses, and thus two questions rise:

• Can we include in each PDE value an amount of pulses that is considered "noise"?
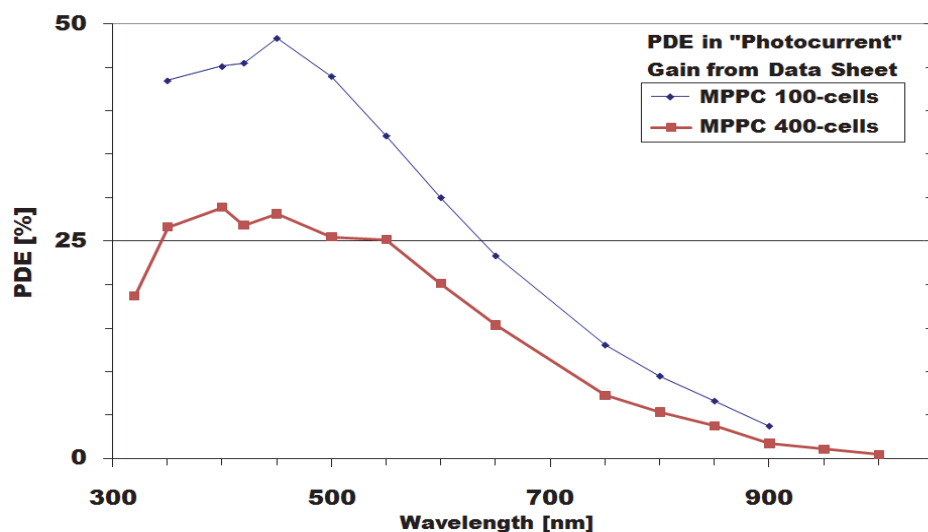• Can we say that the obtained PDE values are accurate?

Fig. 19. PDE plots of the two Hamamatsu G-APDs: the 100-cells MPPC and 400-cells MPPC by using the "Photocurrent" method.

If it is impossible to discriminate the extra pulses with respect to the real signal, probably the photocurrent method may lead to overestimated PDE values, and will be better to use another method that can discriminate the real photo-events from extra pulses.

9.2 Photon counting method

The "Photon counting" method is based on measuring the G-APDs count rate due to the real photo-events and comparing it to the photocurrent measured by the ammeter converted into number of electrons per second. The formula of this method is:

$$\text{PDE} = \left[\left(\text{CR}_{\text{Det}} - \text{CR}_{\text{DarkDet}}\right) / \left(\text{I}_{\text{PhD}} - \text{I}_{\text{DarkPhD}}\right) \times \text{PDE}_{\text{PhD}}\right] \times e^- \times \left(\text{A}_{\text{PhD}} / \text{A}_{\text{Det}}\right) \qquad (3)$$

Where CR_{Det}-$\text{CR}_{\text{DarkDet}}$ is the measured count rate, e- is the electron charge and I_{PhD}-$\text{I}_{\text{DarkPhD}}$, PDE_{PhD}, A_{PhD}/A_{Det} are the same as on formula (2).

By using this method the afterpulse and the cross-talk can be characterized and taken into account in the right way, in fact we can set the threshold at a convenient value and can acquire the signal at a selected time (by varying the time length of the digital output pulse from the discriminator) away from the eventual afterpulse contribution. The first step to carry out the PDE measurement is to analyse the count rates as a function of the threshold. As seen in Fig.16 of section 7, a threshold equivalent to 0.5 photons can be selected as this value is in a safe plateau region. In the tested devices we found that the afterpulse probability is not appreciable after ≈100ns and thus we settled the output logic signal duration from the discriminator longer than this value. We counted the number of pulses per unit time both in dark conditions (~ 600 KCnts/s for the 100-cells MPPC, ~ 500 KCnts/s for the 400-cells MPPC, ~ 500 KCnts/s for the 100-cells STMicroelectronics device) and with monochromatic light conditions (photon signal ranging from ~ 100 KCnts/s to ~ 500 KCnts/s), recording at the same time the light level seen by the reference detector, for several wavelengths. We also carefully tuned the light intensity to keep at negligible levels the pile-up probability. As an example here the analysis made on both the STMicroelectronics and Hamamatsu 100-cells G-APDs is presented. For both devices we evaluated the PDE by measuring all the contributing signals, noise and photons with two gate logic signal durations and accounted for the dead time. For the STMicroelectronics we selected the duration of 50 ns and 500 ns and the resulting PDE plots are shown in Fig. 20, while for the Hamamatsu device we selected the duration of 100 ns and 1000 ns and the resulting plots are shown in Fig. 21. The unappreciable difference between the two sets of
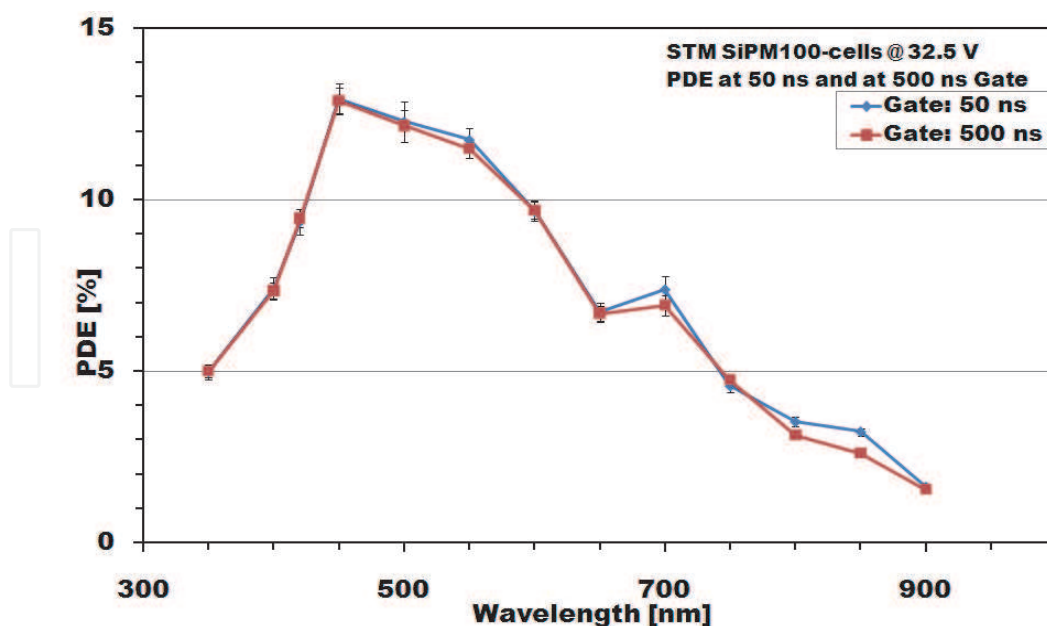

Fig. 20. PDE of the 100-cells SiPM STMicroelectronics device biased at 32.5 V, measured and reconstructed with our method using logic signal durations of 50ns and 500ns respectively. As can be noted the difference between the two sets of measurements is unappreciable, meaning that the afterpulse effect not influence each measure.

measurements, for both G-APDs, demonstrates that the afterpulses are not influent on each measure and strongly supports the correctness of this method.
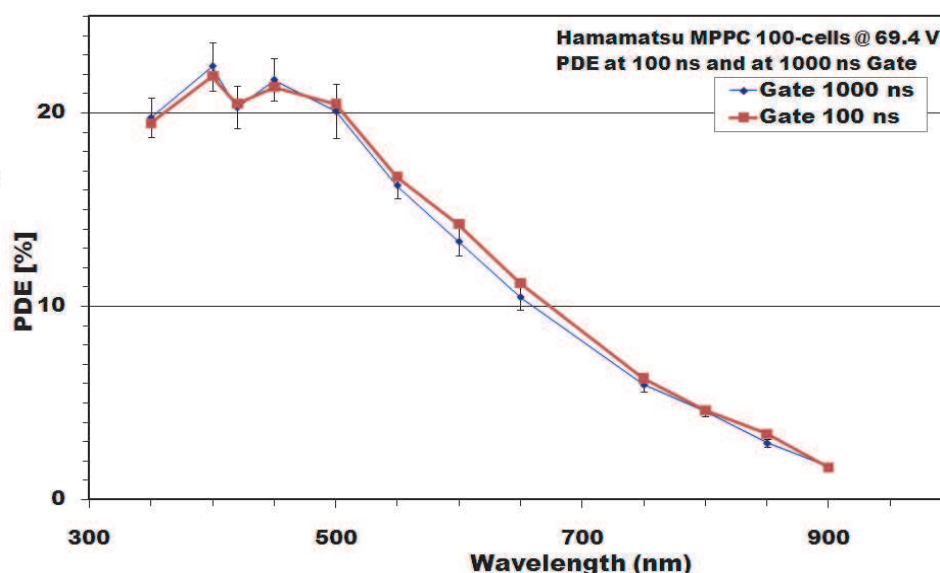

Fig. 21. PDE measured for the Hamamatsu 100 cells biased at 69.4 V using gate signals of 100ns and 1000ns. As can be noted the difference between the two sets of measurements, also in this case, is within the error-bar, meaning that in these measurements the afterpulses are not a problem.

As can be noted from Figs. 20 and 21 the PDE plots of the two G-APDs are quite different specially in the 350 ÷ 450 nm spectral region. This is essentially due to the different technology adopted by the two manufacturers. In the case of Hamamatsu device (that uses the so called p-on-n junction technology) the photons impinging in the first layers of material are absorbed more efficiently than those arriving in the same region of the STMicroelectronics device (that uses the so called n-on-p junction technology).

10. Comparison between "photocurrent" and "photon counting" methods

In order to compare the photocurrent method with the photon counting one, we have plotted in Fig. 22 the PDEs obtained with the two methods for the Hamamatsu MPPC 100-cells.
As can be seen from Fig. 22, the PDE obtained with the photocurrent method is systematically higher than that measured with the photon-counting mode in all the spectral range. Moreover the error-bars associated to the PDE values are very low (not exciding the point itself) demonstrating the high accuracy of measurements and the real difference between the two PDE curves. Unequivocally, Fig. 22 shows that each PDE value obtained using the photocurrent method doubles that of the photon counting operating mode. We, thus have to conclude that the extra noise pulses heavily influence the detector PDE evaluation. A different way that allows us to better clarify the real difference between the two methods, is to represent the two PDE plots as in Fig. 23 where the left axis is used to represent the PDE values obtained with the photocurrent method and the right axis refers to the PDE values obtained in photon counting mode. In order to better understand this figure, it is extremely important to note that the right axis scale (that refers to the photon counting mode) is exactly half of that of the principal axis (that refers to the photocurrent mode).

From the Fig. 23 we can observe that even if the two PDE plots came from different methods, there's an amazing over-position between the two plots. This demonstrates that at each wavelength the PDE values obtained with the two different methods can be related between themselves, and by noting the scale of the left axis respect to right axis, the relation is that each value almost doubles the corresponding. And then, definitively, we can conclude that the PDE of this device in photon counting mode is half of that in which we can't avoid the extra pulses contribute.
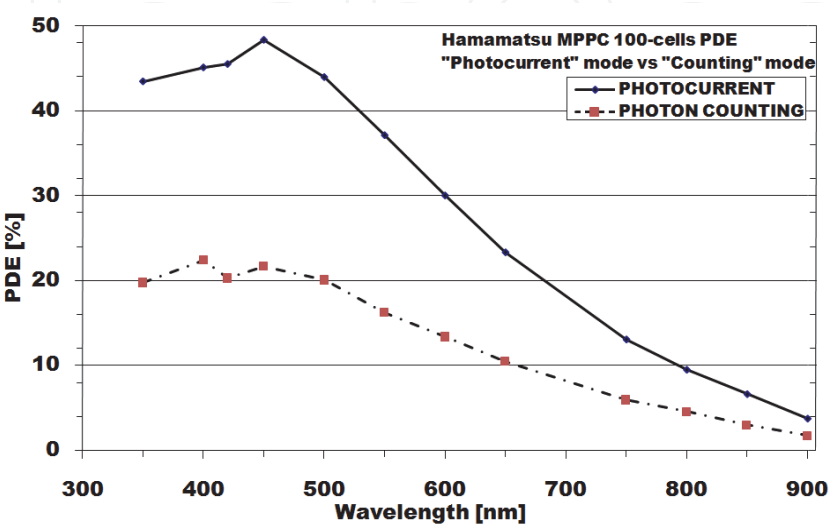
Fig. 22. PDE measurements for a 100-cells Hamamatsu MPPC. The solid line refers to the PDE obtained with the photocurrent method, while the dashed line refers to the PDE obtained with the photon counting technique. Unequivocally the PDE values obtained using the photocurrent method doubles that of the photon counting.
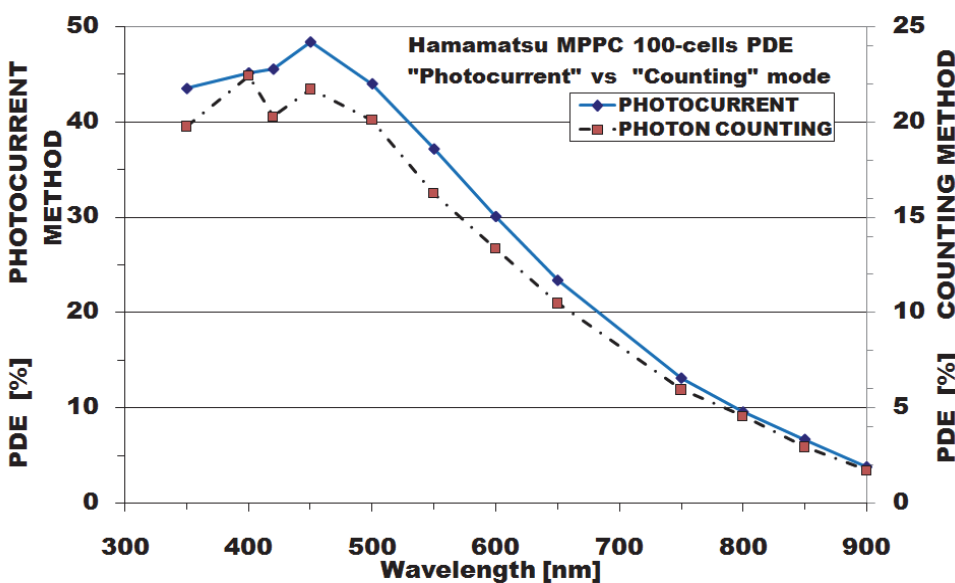

Fig. 23. "Photocurrent" method versus "Photon counting" method. The solid line refers to the PDE (values on the left axis) obtained with the photocurrent method, while the dashed line refers to the PDE (values on the right axis) obtained in photon counting regime. The right axis scale is half of that that refers to the PDE obtained with the photocurrent method.

11. Conclusion

In this chapter, a detailed description of a particular kind of photodiodes able to work in Geiger avalanche mode recently named G-APDs has been described. Starting from a description of the relevant characteristics of the single G-APD we extended to describing the multi-element G-APD as a photodetector constituted by hundreds/thousands of single elements. By discussing in detail the manufacturing technology and the relevant electro-optical characteristics of these devices, we tried to give an idea of the real achievable performance in application such as Nuclear Physics or Astrophysics. The characterisation in terms of noise, and Photon-Detection Efficiency (PDE) has been treated in great detail for both kind of devices together with the adopted experimental setups. Some measurements and results on various single element G-APDs and multi-element G-APDs, manufactured by various companies have been also presented. Finally, emphasis has been given to the developed technique to obtain very accurate PDE measurements based on single photon counting with subtraction of dark noise, and avoiding as much as possible cross-talk and afterpulses. We discussed and compared the two commonly used techniques to measure the PDE, the photocurrent consisting in measuring the photo-generated current in the detector, and the photon counting consisting in measuring the signal considered as number of photons. The comparison between the two methods has pointed out the vulnerability of the photocurrent method that gives PDE values overestimated with respect to those from photon counting. We demonstrated unequivocally that this is essentially due to the fact that the photocurrent technique cannot discriminate the afterpulse and the cross-talk effects. On the contrary, the photon counting method allows to characterize and accurately discriminate the two noise effects providing PDE values quite close to the real ones, but needs to operate in appropriate signal conditions, in fact very fast events can be lost and the total counted events can be lower than those expected. Then we can conclude that the photon counting is a method well suited for PDE measurements because it definitely deals with true photons, reducing as much as possible the contribution of extra pulses.

12. References

S. Billotta et al., JMO, Vol. 56, 273–283 (2009).

G. Bonanno et al., SPIE Proceedings, 2808, p.242 (1996).

R.G. Brown et al., Appl. Opt. 26, 2383 (1987).

P. Buzhan et al., Nucl. Instrum. Methods Phys. Res. A, Accel. Spectrom. Detect. Assoc. Equip., vol. 504, no. 1–3, 48–52, (2003).

S. Cova et al., Appl. Opt. 35, 1956 (1996).

S. Cova et al., Rev. Sci. Instrum. 52, 408 (1981).

B. Dolgoshein et al., Nuclear Instruments and Methods in Physics Research A 563, 368–376 (2006)

P. Finocchiaro et al., IEEE Trans. on Electron Devices, Vol. 55, no. 10, 2757-2764 (2008).

P. Finocchiaro et al., IEEE Trans. on Nucl. Sci., Vol. 56 no. 3, 1033-1041 (2009).

M. Ghioni et al., Rev. Sci. Instrum., vol. 67, no. 10, 3440–3448, (1996).

M. Ghioni and G. Ripamonti, Rev. Sci. Instrum. 62 163 (1991).

V. D. Kovaltchouk et al., Nucl. Instrum. Methods Phys. Res. A, Accel. Spectrom. Detect. Assoc. Equip., vol. 538, no. 1–3, 408–415 (2005).

M. Mazzillo et al., Nucl. Instrum. Methods A Vol. 591, 367–373 (2008).

M. Mazzillo et al., Sens. Actuators A, Vol.138, 306–312 (2007).

C. L. Melcher and J. S. Schweitzer, IEEE Trans. Nucl. Sci., vol. 39, no. 4, 502–505 (1992).

C. Piemonte, Nucl. Instrum. Methods Phys. Res. A, Accel. Spectrom. Detect. Assoc. Equip., vol. 568, no. 1, 224–232 (2006).

F Zappa et al., JMO Vol. 54, 163-189 (2007).
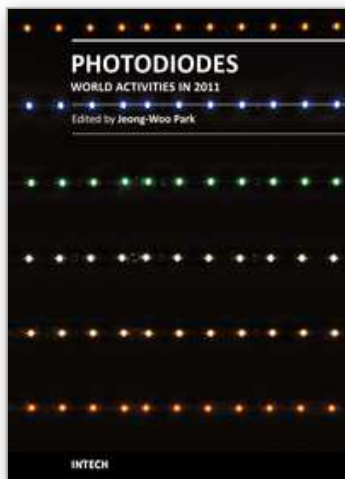
Photodiodes - World Activities in 2011

Edited by Prof. Jeong Woo Park

Photodiodes or photodetectors are in one boat with our human race. Efforts of people in related fields are contained in this book. This book would be valuable to those who want to obtain knowledge and inspiration in the related area.

How to reference

In order to correctly reference this scholarly work, feel free to copy and paste the following:

INTECH
open science | open minds